Elastic pp̄ scattering amplitude at 1.8 TeV and determination of total cross section

A. K. Kohara, E. Ferreira, and T. Kodama

Instituto de Física, Universidade Federal do Rio de Janeiro, Caixa Postal 68528, 21945-970 Rio de Janeiro, Rio de Janeiro, Brazil
(Received 7 August 2012; published 20 March 2013)

The data on pp̄ elastic scattering at 1.8 and 1.96 TeV are analyzed in terms of real and imaginary amplitudes, in a treatment with high accuracy, covering the whole t range, and satisfying the expectation of dispersion relation for amplitudes and for slopes. A method is introduced for the determination of the total cross section and the other forward scattering parameters and to check compatibility of E-710, CDF, and the recent D0 data. Slopes B_R and B_I of the real and imaginary amplitudes, treated as independent quantities, influence the amplitudes in the whole t range and are important for the determination of the total cross section. The amplitudes are fully constructed, and a prediction is made of a marked dip in $d\sigma/dt$ in the $|t|$ range 3–5 GeV^2 due to the universal contribution of the process of three-gluon exchange.

I. INTRODUCTION

The precise knowledge of total cross section and scattering amplitudes in pp and pp̄ elastic scattering at high energies is essential for understanding the QCD interactions and hadronic structure, and also for the parametrization and extrapolation of the total cross section that may pass through the LHC measurements [1] and go up to the study of ultrahigh-energy phenomena in cosmic rays [2]. However, at high energies, the small size of the ratio ρ of the real to the imaginary parts of amplitudes at $t = 0$, together with the absence of data for small $|t|$, turn the extrapolations towards the limit $|t| \rightarrow 0$ very delicate. It is of fundamental importance to well characterize the scattering amplitudes that are used to determine forward slopes and the total cross section.

It is universally understood that the real and imaginary amplitudes in pp and pp̄ elastic scattering at high energies reflect the nonperturbative QCD dynamics, determined by overall features of the proton and antiproton structures. Regge-like behavior characterizes the s and t dependencies at large s and small $|t|$. There appears to be a dip or an inflection point in the differential cross section $d\sigma/dt$, near the occurrence of a zero in the imaginary part, and the detailed shape around this region is influenced by the magnitude, sign, and form of the real part. An analysis of the interplay of real and imaginary amplitudes is necessary to reproduce with accuracy the behavior of the $|t|$ dependence.

An analytical representation for the amplitudes valid for the whole $|t|$ range must contain implicitly the exponential decrease of the amplitudes in the very forward region; account for their curvatures, zeros, signs, and magnitudes; and also should contain the ingredients that describe the universal power behavior at large $|t|$ due to the three-gluon exchange contribution. The determination of the detailed properties of the real and imaginary parts is crucial for the accurate description of the observed differential cross section. The analytical forms of the amplitudes used in the

present work extend previous studies at the ISR energies [3] based on the stochastic vacuum model [4]. More recently, with additional controls offered by dispersion relations for amplitudes and for slopes [5], the method has been applied to the recent 7 TeV data from LHC [6].

The present work extends the previous studies to give a high-precision description of the data on pp̄ elastic scattering at 1.8 TeV [7,8] and 1.96 TeV [9], consistently covering the forward and the backward regions. This work is particularly opportune in view of the publication of the new measurements at 1.96 TeV covering a large $|t|$ range by the D0 Fermilab experiment [9]. Our framework offers the opportunity of an investigation of the connection and compatibility of the previous 1.8 TeV and the recent 1.96 TeV data. It should be stressed here that in the analysis of the data, we use information from forward dispersion relations to control parameters of the full description and particularly emphasize the importance of the difference of the slope parameters, B_R and B_I, of the real and imaginary parts. It is commonly assumed in the analysis of data that these slopes are the same, but this is wrong theoretically, a fact that is often overlooked due to the small value of the ρ parameter. However, to describe consistently the scattering amplitude for the full $|t|$ range, the difference of slopes is crucial, since a description that covers the large t region constrains the quantities of the forward range. This is particularly true and important for the real amplitude that is small with respect to the imaginary part in the forward direction, but not at large $|t|$. Actually, in our analysis the differential cross section at high $|t|$ is dominated by the real part [3,6].

In the very large $|t|$ domain, the perturbative QCD effects become dominant, forming a power decreasing tail in the differential cross section that was first measured at 27.4 GeV [10]. It is known that this tail is energy independent and formed by a real contribution due to three-gluon exchange [11], with opposite signs for pp and pp̄ (positive in pp and negative in pp̄) scattering. In our approach the universality of the perturbative 3-gluon

exchange process is incorporated explicitly, determining the asymptotic behavior of the real amplitude. It is thus interesting to investigate the connection of the measured points at 1.8 and 1.96 TeV with the assumption of the universal tail. We show that the perturbative amplitude leads to a striking prediction for the behavior of the cross section. In $p\bar{p}$ scattering, when added to the nonperturbative positive real part, the perturbative term creates a third zero located in the region about $|t| \approx 3$–4 GeV^2. As the imaginary part is less important in this domain, a marked dip is caused by this cancellation.

Our treatment of the whole data with overall high precision leads to definite prediction for the forward scattering parameters in the context of one analytical form for each amplitude. We thus have a determination of the total cross section σ and of the quantities ρ, B_I, and B_R, while still allowing curvatures of the scattering amplitudes. When data are not available at very low $|t|$, the existence of curvatures prevents accurate analysis in terms of pure exponential forms, so that the determination of σ becomes model dependent. Based on our experience with other energies, we here advocate that the determination of the scattering parameters based on the full data is necessary, since it incorporates realistic properties of the amplitudes.

We organize the present work as follows. In Sec. II, we present the analytical forms of the scattering amplitudes that describe the whole $|t|$ range and the necessary quantities are defined, with a discussion of the role of the universal perturbative contribution for large $|t|$. In Sec. III, the analysis of the 1.8–1.96 TeV data with determination of all quantities is presented. In Sec. IV, we present the amplitudes and compare our results with other theoretical models. In Sec. V, we discuss our predictions and proposals.

II. GENERAL FORM OF FULL t SCATTERING AMPLITUDE

In the treatment of elastic pp and $p\bar{p}$ scattering in the forward direction, with amplitudes approximated by pure exponential forms, the differential cross section is written

$$\frac{d\sigma}{dt} = \pi(\hbar c)^2 \left\{ \left[\frac{\rho\sigma}{4\pi(\hbar c)^2} e^{B_R t/2} + F^C(t)\cos(\alpha\Phi) \right]^2 \right.$$
$$\left. + \left[\frac{\sigma}{4\pi(\hbar c)^2} e^{B_I t/2} + F^C(t)\sin(\alpha\Phi) \right]^2 \right\}, \quad (2.1)$$

where $t \equiv -|t|$ and we assume different values for the slopes B_I and B_R of the imaginary and real amplitudes. In the following discussion, we use the unit system where σ is in mb (milibarns) and energy in GeV, so that $(\hbar c)^2 = 0.389$ mb GeV^2.

The Coulomb amplitude $F^C(s, t)$ enters for pp/$p\bar{p}$ with the form

$$F^C(s, t)e^{i\alpha\,\Phi(s,t)} = (-/+)\frac{2\alpha}{|t|} e^{i\alpha\,\Phi(s,t)} F^2_{\text{proton}}(t), \quad (2.2)$$

where α is the fine-structure constant, $\Phi(s, t)$ is the Coulomb phase, and the proton form factor is written

$$F_{\text{proton}}(t) = [0.71/(0.71 + |t|)]^2. \quad (2.3)$$

Contradicting expectations from dispersion relations [5], in usual treatments of the data no distinction is made between B_R and B_I slopes, and $B_R \neq B_I$ requires a more general expression for the Coulomb phase [6], which is used in the present work. Other evaluations of the Coulomb phase [12] do not change meaningfully the results of this paper.

In elastic pp and $p\bar{p}$ scattering at all energies above $\sqrt{s} = 19$ GeV, the real and imaginary amplitudes have zeros located in ranges $|t| \approx (0.1$–$0.3)$ GeV^2 and $|t| = (0.5$–$1.5)$ GeV^2, respectively, and the use of exponential forms beyond a limited forward range leads to inaccurate determination of the characteristic forward scattering parameters σ, ρ, B_I, and B_R. To obtain a precise description of the elastic $d\sigma/dt$ data for all $|t|$, we introduce amplitudes with forms [3,6]

$$T_R(s, t) = \alpha_R(s)\exp(-\beta_R(s)|t|) + \lambda_R(s)\Psi_R(\gamma_R(s), t)$$
$$+ \sqrt{\pi}F^C(t)\cos(\alpha\Phi) \quad (2.4)$$

and

$$T_I(s, t) = \alpha_I(s)\exp(-\beta_I(s)|t|) + \lambda_I(s)\Psi_I(\gamma_I(s), t)$$
$$+ \sqrt{\pi}F^C(t)\sin(\alpha\Phi), \quad (2.5)$$

with the shape functions

$$\Psi_K(\gamma_K(s), t) = 2e^{\gamma_K}\left[\frac{e^{-\gamma_K\sqrt{1+a_0|t|}}}{\sqrt{1+a_0|t|}} - e^{\gamma_K}\frac{e^{-\gamma_K\sqrt{4+a_0|t|}}}{\sqrt{4+a_0|t|}} \right],$$
$$(2.6)$$

where $K = R$ for the real amplitude and $K = I$ for the imaginary amplitude. Here, we have eight quantities, α_I, β_I, γ_I, λ_I, α_R, β_R, γ_R, λ_R, that determine the nonperturbative amplitudes. γ_K is dimensionless, while α_K, λ_K, and β_K are in GeV^{-2}. These forms have been developed in the application of the stochastic vacuum model to pp and $p\bar{p}$ elastic scattering [3], and the fixed quantity $a_0 = 1.39$ GeV^{-2} is related to the square of the correlation length of the gluon vacuum expectation value [$a = (0.2$–$0.3)$ fm] [4].

From the above expression, we can express the total cross section $\sigma(s)$, the ratio ρ of the real to imaginary amplitudes, the slopes $B_{R,I}$ of the amplitudes at $t = 0$, and the differential cross section $d\sigma/dt$ as

$$\sigma(s) = 4\sqrt{\pi}(\hbar c)^2(\alpha_I(s) + \lambda_I(s)), \quad (2.7)$$

$$\rho(s) = \frac{T_R(s, t=0)}{T_I(s, t=0)} = \frac{\alpha_R(s) + \lambda_R(s)}{\alpha_I(s) + \lambda_I(s)}, \quad (2.8)$$

$$B_K(s) = \frac{1}{T_K(s,t)} \frac{dT_K(s,t)}{dt} \bigg|_{t=0}$$
$$= \frac{1}{\alpha_K(s) + \lambda_K(s)} \bigg[\alpha_K(s)\beta_K(s)$$
$$+ \frac{1}{8} \lambda_K(s) a_0 (6\gamma_K(s) + 7) \bigg], \qquad (2.9)$$

$$\frac{d\sigma}{dt} = (\hbar c)^2 |T_R(s,t) + i T_I(s,t)|^2. \qquad (2.10)$$

We have thus defined the form of the amplitudes for all t at each energy. The parameters must be determined by a phenomenological analysis of the data, with control from dispersion relations for amplitudes and for slopes. The forms of Eqs. (2.4), (2.5), and (2.6) are able to describe the imaginary and real amplitudes at all energies, with consistency in their features (magnitudes, signs, locations of zeros), and with smoothness in the energy dependence of the parameters. Values of ρ and B_R must be related with σ and B_I respecting dispersion relations. This description represents the nonperturbative QCD dynamics that is responsible for the soft elastic hadronic scattering. They effectively account for the terms of Regge and eikonal phenomenology that determine the process of $|t|$ ranges up to about $|t| \approx 2.0$ GeV^2.

This representation of the scattering amplitudes has been used successfully to reproduce the data at ISR [3] and LHC energies [6]. In these applications, it was found that the imaginary amplitude presents one zero located in the range (0.5–1.5 GeV^2), while the real amplitude presents one zero at low $|t|$ ($|t| < 0.3$ GeV^2), according to a theorem by Martin [13], and a second zero whose location determines the shape of $d\sigma/dt$ around the dip (or inflection point). As a general behavior, we have that the imaginary part, Eq. (2.5), is negative and the real part, Eq. (2.4), is positive for $|t|$ larger than 1.5 GeV^2. These simple features are general and all data are described accurately.

It is observed that after the dip (or inflection point) the behavior of the differential cross sections becomes increasingly energy independent. The elastic pp experiment at $\sqrt{s} = 27$ GeV [10] has measured the range from 5.5 to 14.2 GeV^2 and these are the only measurements at such high values of $|t|$. This distribution at high $|t|$ shows remarkable universality: at all energies $\sqrt{s} = 23.5$, 30.7, 44.7, 52.8, and 62.5 GeV, namely, at all energies where measurements have reached the intermediate $|t|$ region, $d\sigma/dt$ approaches the same set of points of the 27.4 GeV experiment.

The observed $d\sigma/dt$ at the tail has a dependence of form $1/|t|^8$, and has been explained by Donnachie and Landshoff [11] as being of perturbative origin, due to a contribution of the three-gluon exchange. This term is real and has an amplitude of the form

$$A(s,t)_{ggg} = -\frac{N}{|t|} \frac{5}{54} \bigg[4\pi\alpha_s(|\bar{t}|) \frac{1}{m^2(|\bar{t}|) + |\bar{t}|} \bigg]^3, \qquad (2.11)$$

where

$$\alpha_s(|\bar{t}|) = \frac{4\pi}{(11 - \frac{2}{3}N_f)[\log(\frac{m^2(|\bar{t}|) + \bar{t}}{\Lambda^2})]} \qquad (2.12)$$

is the strong coupling constant and $m(|t|)$ is the gluon effective mass [14]. The factor 3 in $\bar{t} \approx (\sqrt{t}/3)^2$ comes from the assumption that each gluon carries one third of the momentum. The normalization factor N is negative and determined by the nucleon structure. To extend our description to include the very high $|t|$ range of this form, we introduce a term $R_{ggg}(t)$, writing

$$T_{R(\text{tail})}(s,t) = \alpha_R(s) \exp(-\beta_R(s)|t|) + \lambda_R(s)\Psi_R(\gamma_R(s),t)$$
$$+ \sqrt{\pi} F^C(t) \cos(\alpha\Phi) + R_{ggg}(t), \qquad (2.13)$$

where $R_{ggg}(t)$ is chosen so that the differential cross section to be dominated by a term of the form $|t|^{-8}$ for large $|t|$ values (say above 2.5 GeV^2), while for small $|t|$ the amplitude is determined by the original nonperturbative expression. The perturbative three-gluon exchange has opposite signs for pp and pp̄ scattering, being positive for pp and negative for pp̄. We then take the following expression:

$$R_{ggg}(t) \equiv \pm 0.45 t^{-4} (1 - e^{-0.005|t|^4})(1 - e^{-0.1|t|^2}), \qquad (2.14)$$

where the signs $\pm$ apply to the pp and pp̄ amplitudes, respectively. The factor 0.45 is chosen to reproduce the Faissler measurements and the last two factors are written to suppress smoothly the perturbative contribution for small $|t|$. The transition region from 2 to 5 GeV^2 contains information on the nature and superposition of nonperturbative and perturbative contributions, and must be investigated, both experimentally and theoretically. In the pp̄ case, the negative sign may lead to a zero in the real amplitude, with an interesting consequence for the form of $d\sigma/dt$.

The change in sign of this contribution for pp and pp̄ amplitudes leads to a very interesting consequence for pp̄ case, which will be discussed in Sec. IV.

III. ANALYSIS OF ELASTIC pp̄ DATA AT 1.8 TEV

The available experimental data on differential cross section of pp̄ elastic scattering at 1.8 TeV are as follows:
  (i) N = 51 points in the interval $0.00339 \leq |t| \leq 0.627$ (in GeV^2) from the Fermilab E-710 experiment published by N. Amos *et al.* [7] in 1990.
  (ii) N = 26 points in the interval $0.0035 \leq |t| \leq 0.285$ (in GeV^2) from the Fermilab CDF experiment published by F. Abe *et al.* [8] in 1994.
To these data we may now add the results of the experiment at 1.96 TeV.

(i) N = 17 points in the interval $0.26 \leq |t| \leq 1.20$ (in GeV^2) from the Fermilab D0 experiment published by V. M. Abazov *et al.* [9] in 2012.

In order to use the last set together with the former two sets, in this paper we use the reduction factor $(1.8/1.96)^{0.3232} = 0.973$ obtained as correction of energy effect from 1.96 to 1.8 TeV according to Regge phenomenology [15]. As the $|t|$ range involved is small we neglect the $|t|$ dependence of this factor. In the following, we refer to these converted data as "1.96 TeV data."

The data are shown in Fig. 1. They do not cover a low enough $|t|$ range for a precise treatment in terms of exponential forms for the amplitudes, or even less, for the differential cross section. Besides, there is a discrepancy of values in the data from the two independent experiments, exhibited in Fig. 1, which has lead to a 20 year old duplicity of values for the total cross section, which has seriously affected the efforts for a global description of the energy dependence of the total cross section.

We recall values of the scattering parameters that are found in original papers by the following experimental groups:

(i) E-710 experiment [16]: $\rho = 0.140 \pm 0.069$, $B = 16.99 \pm 0.47$ GeV^{-2}, $\sigma = 72.8 \pm 3.1$ mb.

(ii) CDF experiment [17]: $B = 16.98 \pm 0.25$ GeV^{-2}, $\sigma = 80.03 \pm 2.24$ mb.

In the present work we analyze carefully this duplicity using a full t analytic description of the real and imaginary amplitudes with help of the new large $|t|$ data from the 1.96 TeV experiment. As much as possible, we deal with all experimental information together in a unified analysis. For this purpose, we group the data in three different sets.

(i) SET I: The 1.96 TeV data (converted) give a natural and smooth connection with the E-710 data (basically they come from the same experimental group); there is some superposition in the extreme ends, where we select the more recent data, that have smaller error bars. We thus join 35 points with $3.39 \times 10^{-2} \leq |t| \leq 0.247$ GeV^2 from E-710 with 17 points from D0, to form a combined data SET I (called STANDARD), with N = 52 points in the range $0.00339 \leq |t| \leq 1.2$ GeV^2.

(ii) SET II: We observe that there is a good convergence of the large $|t|$ end points of the CDF spectrum with the beginning of the recent D0 points. This is a welcome surprise, and suggests the consistent construction of a combined set from the two groups, with N = 26 and the N = 17 points, respectively. Actually, to select points in the range where there is superposition, and simultaneously to obtain a clearer smooth connection, we exclude the last 5 CDF points that present a rather scattered behavior (observe Fig. 1). We thus build SET II here (called HYBRID), with N = 21 + 17 = 38 points. The assemblage is shown in Fig. 2. The construction of this HYBRID SET II is motivated by the consideration that the apparently irreconcilable discrepancy between the E-710 and CDF experiments that exists in the low and mid $|t|$ range need not imply that they are incompatible for larger $|t|$. Our description aims at representations of $d\sigma/dt$ covering all $|t|$ spectrum, and this hybrid connection is very important.

(iii) SET III: In a third construction, we investigate what comes out from our full $|t|$ description if we put all
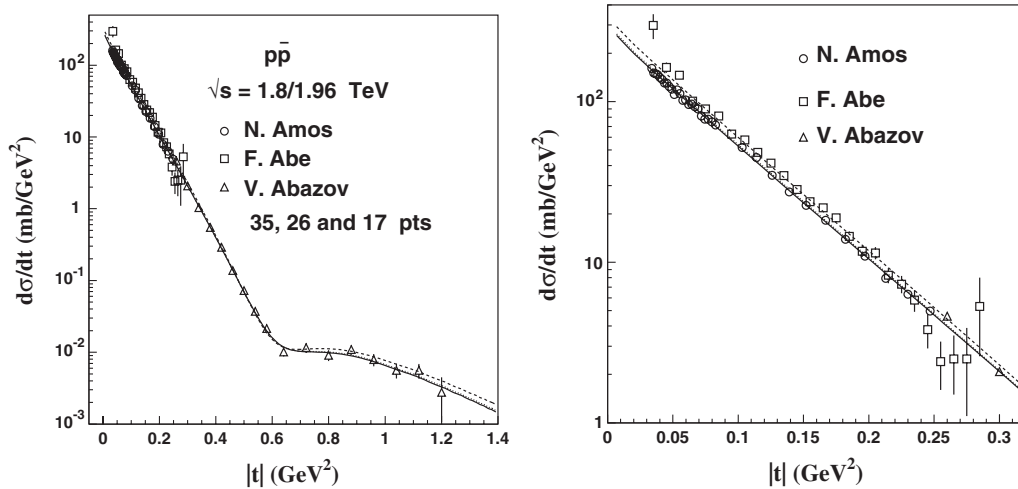

FIG. 1. Data of p$\bar{\text{p}}$ scattering at 1.8 and 1.96 TeV [7–9], taken in the E-710, CDF, and D0 experiments in Fermilab. The D0 data are multiplied by a reducing factor 0.973 to take into account the energy difference (see the text). The E-710 data [7] are restricted to the first 35 points (open circles) due to superposition with the recent D0 data (open triangles) of the same experimental group. The plot in the right-hand side (rhs), concentrated in the forward part, exhibits clearly the known discrepancy between the two experiments in the low $|t|$ region. The solid, dashed, and dotted lines represent, respectively, our best descriptions for data sets I, II, and III constructed from the combination of three data points available, as described in the text. The dotted line is hidden under the solid line.
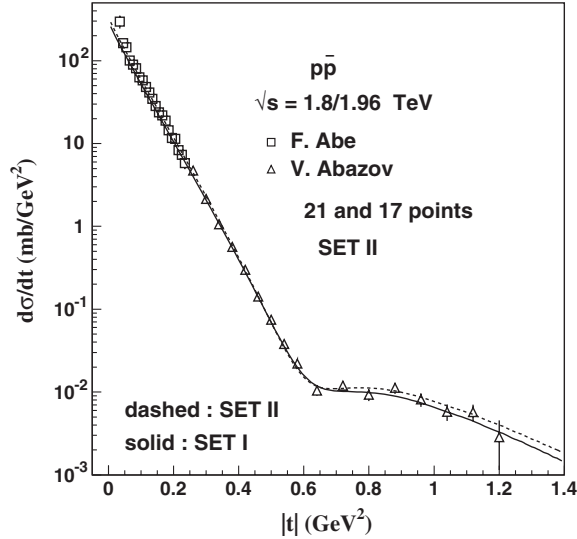
FIG. 2. HYBRID SET. Combination of N = 21 points from CDF (open squares) with 17 points from D0 (open triangles). The last 5 points of CDF data (see Fig. 1) are excluded to exhibit more clearly a smooth connection, and this is done also numerically in fittings with SET II (38 points). The E-710 points do not enter in this SET II. Solid line: Fit of SET I, for comparison. Dashed line: Fit of SET II. Although the lines of the two solutions are visually very close, the limits $|t| \to 0$ lead to different values of σ, given in Table I and shown in close-up in Fig. 3.

data together on the same footing, merging the N = 52 points of SET I with the N = 26 CDF basis. We thus form a GLOBAL SET III, with N = 78 points.

We fit $d\sigma/dt$ for the three data sets described above, using Eqs. (2.4), (2.5), (2.6), and (2.10) of our representation. In the fitting procedure, in principle all 8 parameters are treated independently to minimize χ^2, but we find that some parameters can be chosen with common values to all data sets without sensitive changes in the solutions. They are

$$\alpha_I = 11.620 \pm 0.024 \text{ GeV}^{-2}, \qquad \beta_R = 1.10 \text{ GeV}^{-2},$$

$$\rho = 0.141 \pm 0.002, \qquad B_I = 16.76 \pm 0.04 \text{ GeV}^{-2},$$

$$B_R = 26.24 \pm 0.39 \text{ GeV}^{-2}. \qquad (3.1)$$

We remark that the usual quantity B (slope of $d\sigma/dt$) is not the same as B_I. The relation is

$$B = \frac{B_I + \rho^2 B_R}{1 + \rho^2} \qquad (3.2)$$

and we then obtain $B = 16.94 \text{ GeV}^{-2}$, remarkably close to the values of the experimental groups (16.99 ± 0.47 and $16.98 \pm 0.25 \text{ GeV}^{-2}$ for the E-710 [16] and CDF [17] groups, respectively).

The results of the fittings with respect to the other free parameters are given in Table I, together with some characteristic features of the solutions. The corresponding curves representing these fittings of $d\sigma/dt$ are shown in Figs. 1–3.

It is important to observe that the discrepancy between the CDF and E-710 data shown in the rhs of Fig. 1 becomes smaller as $|t|$ increases and both sets of data seem to connect smoothly to the D0 data, as seen in Fig. 3. That is, the well-known contradiction between E-710 and CDF data becomes less serious as $|t|$ increases, and the D0 data help to point out the connection. Our global $|t|$ analysis helps to describe this connection.

We recall that the above analysis is based on analytical expressions for the scattering amplitudes applied to all $|t|$. In the present 1.8 TeV case, the integrated use of all $|t|$ data is crucial since there are no data points in the very forward range, 10^{-3} to 10^{-2} GeV^2, and the pure exponential forms are not at all reliable. Due to the very large energy gaps in the experimental data, this energy region $\sqrt{s} = 1.8/1.96$ TeV is extremely important for the determination of the energy dependence of the total cross section, $\sigma(s)$ and hence for its extrapolation for ultrahigh energies treated by fundamental theorems.

To show the importance of the use of the full $|t|$ amplitudes and full $|t|$ data together, we test toy fits of the forward data of E-710 (35 points) and CDF (21 points) experiments. The E-710 data are fitted with essentially the same parameters as the full SET I, and this shows their nearly perfect coherence, with the E-710 and D0 data matching very well when described by our full $|t|$ amplitudes. However, the separate treatment of the 21 points of

TABLE I. Characteristic quantities of the all t representation for the amplitudes. Common values for all sets: $\rho = 0.141 \pm 0.002$, $B_I = 16.76 \pm 0.04 \text{ GeV}^{-2}$, $B_R = 26.24 \pm 0.39 \text{ GeV}^{-2}$, $\alpha_I = 11.620 \pm 0.024 \text{ GeV}^{-2}$, and choice of $\beta_R = 1.10 \text{ GeV}^{-2}$. The remaining free parameters are β_I, λ_R, σ. The error bars are given by the CERN Minuit Program in each case with all parameters fixed, except the one whose error bar is evaluated. Open correlations among parameters may lead to larger error bars. SET I is built with E-710 (35 points) and D0 (17 points) data. SET II is built joining CDF (21 points) and D0 (17 points). The complete SET III puts together CDF (26 points), E-710 (35 points), and D0 (17 points) data. $|t|_{\text{infl}}$ is the position of the inflection point in $d\sigma/dt$. $\langle\chi^2\rangle$ is the average value of the squared relative theoretical/experimental deviations.

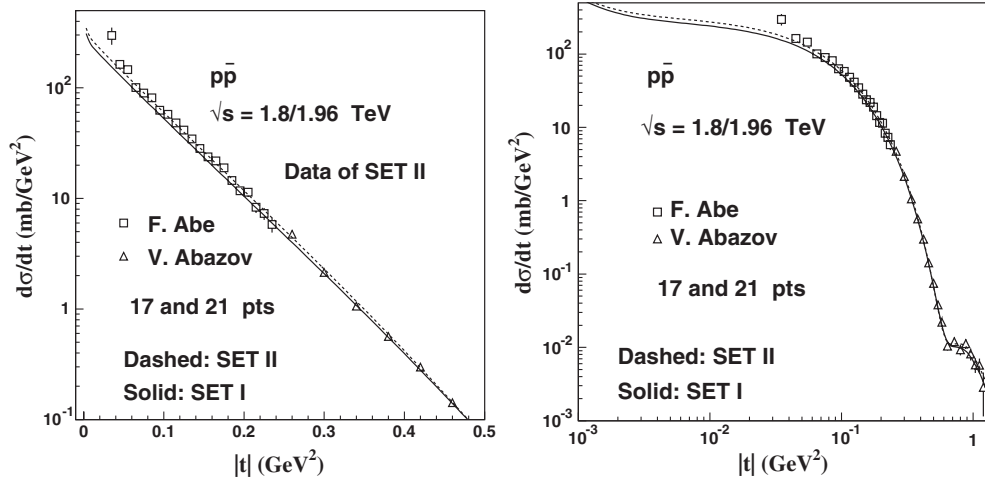| SET	N points	β_I GeV^{-2}	λ_R GeV^{-2}	$|t|_{\text{infl}}$ GeV^2	$(d\sigma/dt)_{\text{infl}}$ mb/GeV^2	σ (el) mb	σ mb	$\langle\chi^2\rangle$
I	52	3.7785 ± 0.0078	3.6443 ± 0.0093	0.745	0.01013	16.67	72.76 ± 0.13	0.7661
II	38	3.5686 ± 0.0186	3.8645 ± 0.0093	0.727	0.01114	18.92	77.63 ± 0.44	1.4961
III	78	3.7441 ± 0.0080	3.6784 ± 0.0096	0.741	0.01029	17.02	73.54 ± 0.20	2.6591

FIG. 3. Data of SET II (21 points from CDF and 17 points from D0 experiment), with plots that enhance the forward range. Note the smooth connection of the highest $|t|$ CDF points with the recent D0 data. The solid and dashed lines refer to the fitting solutions obtained with sets I and II, respectively, with parameters given in Table I. In spite of the apparent proximity, the lines lead to remarkably different values for the total cross section. The solution for SET III falls between these two drawn lines (see dotted line in Fig. 1) and is not included here to keep clarity.

the CDF data leads to values of $\beta_I = 3.7280 \text{ GeV}^{-2}$, $\lambda_R = 3.3060 \text{ GeV}^{-2}$ and $\sigma = 79.00 \pm 0.57$ mb that are different from those of the combined SET II in Table I, and this solution has a disastrous behavior for large $|t|$. Thus, we conclude that in our model the use of the pure CDF points for the determination of the very forward quantities seems unreliable if it is not controlled by the D0 points of the larger $|t|$ domain. Thus, in our analysis the construction of SET II is essential for the treatment of the CDF data.

IV. PROPERTIES OF AMPLITUDES

It is the general property of our scheme that the non-perturbative amplitudes fall off rapidly after $|t| \approx 1.5 \text{ GeV}^2$, with the magnitude of the positive real part becoming dominant over the negative imaginary part for $|t|$ larger than about 2.5 GeV^2. The imaginary amplitude has only one zero located near the inflection point of $d\sigma/dt$, while the real part has a first zero at small $|t|$, obeying Martin's theorem [13], and a second zero located after the imaginary zero. As the nonperturbative real part decreases, the perturbative tail remains, giving to the differential cross section the characteristic shape $1/|t|^8$, discussed by Donnachie and Landshoff [11]. Such a general aspect of the scattering amplitudes have been well verified at ISR and LHC energies [3,6]. The present analysis at 1.8 TeV data repeats this general behavior, as exhibited in Fig. 4.

A. Role of perturbative tail in p$\bar{\text{p}}$ scattering

The universal (energy independent) perturbative 3-gluon exchange process [11], given by Eq. (2.14), contributes in p$\bar{\text{p}}$ scattering with a negative sign, which leads to an interesting prediction. As mentioned above, the

nonperturbative real amplitude is positive in the transition region, and the inclusion of the negative tail amplitude leads eventually to its cancellation and the creation of a third real zero (see Table II). This mechanism is shown in the rhs of Fig. 4, where we draw two curves for the real amplitude with a solid line and a dashed line corresponding, respectively, to the presence and absence of perturbative contribution.

As the imaginary part is not dominant in this region, a marked dip may be observed in $d\sigma/dt$. This is shown in Fig. 5. In this figure (rhs), we also show with a dotted line the behavior of cross section with nonperturbative amplitudes only, without the effect of perturbative tail.

The precise form of this dip-bump structure created by the perturbative tail depends sensitively on the values of model parameters (such as β_R) that govern the properties of the transition domain. Unfortunately, the existing data stops at about $|t| = 1.2 \text{ GeV}^2$, leaving the higher $|t|$ region without information to fix the connection with the range of the perturbative tail. Thus, the parameter β_R cannot be fixed accurately, and as its value is crucial for the prediction of the position and depth of a dip in the transition region for p$\bar{\text{p}}$ scattering at 1.8 TeV, we present in Table II two alternative choices, with $\beta_R = 1.10$ and 1.40 GeV^{-2}.

In Table II, are given the values of $|t|$ at the zeros of the amplitudes, and the locations of the dip and bump in $d\sigma/dt$ at large $|t|$ that are due to the contribution of the three-gluon exchange term. The quantity ratio $= (d\sigma/dt)_{\text{bump}}/(d\sigma/dt)_{\text{dip}}$ that informs about the shape of the structure depends strongly on the values of the parameter β_R, that must be determined by the experiment, necessarily with extension of the measured range to higher $|t|$ values. The common parameters are given in Eq. (3.1). The fitting of each solution is needed only to evaluate λ_R.
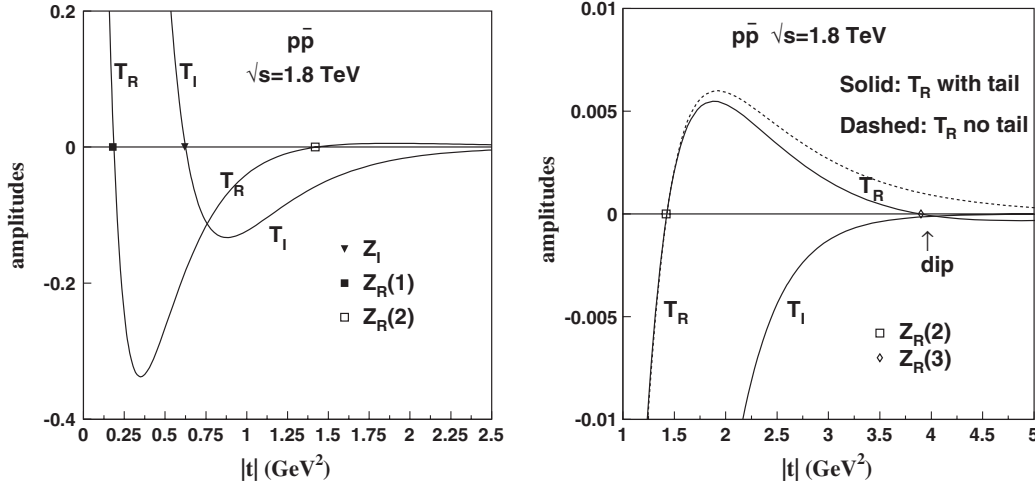
FIG. 4. Amplitudes in p$\bar{\text{p}}$ elastic scattering at $\sqrt{s} = 1.8$ TeV shown in different ranges and scales, described by Eqs. (2.4), (2.5), and (2.6) with parameters determined by phenomenology. The solid lines drawn refer to the solutions for T_R and T_I obtained for SET I. In the $|t|$ range up to about 2 GeV^2 the amplitudes are governed by nonperturbative dynamics and are qualitatively similar for pp and p$\bar{\text{p}}$, with one zero for T_I and two zeros for T_R. T_I remains negative and goes fast to zero, while at $|t| \approx 3$ GeV^2 the nonperturbative T_R is positive and dominates. In p$\bar{\text{p}}$ scattering the negative contribution of the 3-gluon exchange term inverts the sign of T_R, forming a third zero and a marked dip in $d\sigma/dt$, with locations and depths dependent on the detail of the β_R parameter, as shown in Table II.

B. Comparison with the Bourrely-Soffer-Wu (BSW) model

In our work, we emphasize the importance of the determination of the amplitudes that describe the observed quantities in elastic scattering. However, this description is naturally model dependent so that it is interesting to compare our results to those of other models. Results on amplitudes that can be directly compared with ours are given by the model proposed by Bourrely, Soffer, and Wu (hereafter referred to as the BSW model) [18]. Properties of the Pomeron amplitudes [19] are note studied here. The comparison is presented below.

The parameters of the BSW model at 1.8 TeV are

$$\sigma = 73.99 \text{ mb}; \qquad \rho = 0.129;$$

$$B_I = 18.12 \text{ GeV}^{-2}; \qquad B_R = 22.82 \text{ GeV}^{-2};$$

$$Z_I = 0.685 \text{ GeV}^2; \qquad Z_R(1) = 0.275 \text{ GeV}^2;$$

$$Z_R(2) = 2.040 \text{ GeV}^2.$$

Instead of the inflection points, the model gives the first dip and bump for $d\sigma/dt$, with a flat structure, with the values

$$|t|_{\text{dip}} = 0.72 \text{ GeV}^2; \quad |t|_{\text{bump}} = 0.90 \text{ GeV}^2; \quad \text{ratio} = 1.226.$$

TABLE II. Positions of zeros of the real and imaginary amplitudes, locations of the dip and bump at large $|t|$ predicted by the introduction of the perturbative tail of negative sign, and the ratio characterizing the shape of this structure. The parameter β_R, that determines the behavior of the real part at the end of the nonperturbative region, is not tightly determined by the data (that ends at 1.2 GeV^2), and has an important role for the location and depth of the large $|t|$ dip. We present results for two choices of β_R. The parameter λ_R varies in the fits, following the choice of β_R. The quantities ρ, B_I, B_R, α_I are universal, as in Table I. The quantity ratio is $[d\sigma/dt]_{\text{bump}}/[d\sigma/dt]_{\text{dip}}$.

| SET	β_R GeV^{-2}	λ_R GeV^{-2}	Z_I GeV^2	$Z_R(1)$ GeV^2	$Z_R(2)$ GeV^2	$Z_R(3)$ GeV^2	$|t|_{\text{dip}}$ GeV^2	$|t|_{\text{bump}}$ GeV^2	ratio
I	1.10	3.6443	0.6253	0.1771	1.4336	3.8827	3.9456	4.8631	5.4567
I	1.40	3.6328	0.6253	0.1776	1.5884	3.0605	3.4839	4.1212	1.3086
II	1.10	3.8645	0.6156	0.1792	1.2986	4.3159	4.3520	5.3314	8.4118
II	1.40	3.8492	0.6156	0.1799	1.4217	3.3047	3.6434	4.2920	1.3761
III	1.10	3.6784	0.6231	0.1776	1.3987	3.9781	4.0312	4.9580	6.2212
III	1.40	3.6662	0.6231	0.1781	1.5452	3.1181	3.5111	4.1609	1.3442
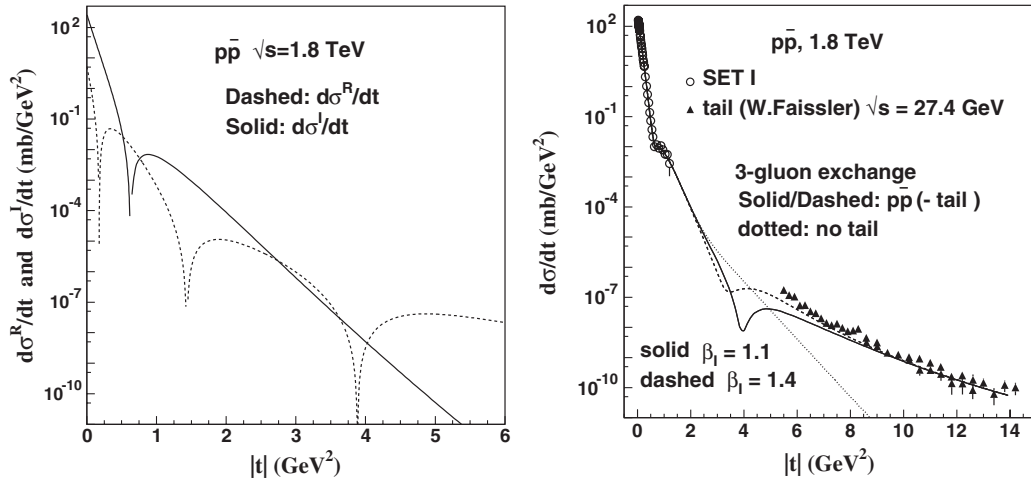
FIG. 5.   The plots show the predictions for the contributions of real $d\sigma^R/dt$ and imaginary $d\sigma^I/dt$ parts of $d\sigma/dt$ in the presence of the real perturbative tail due to 3-gluon exchange. In $p\bar{p}$ scattering, the negative sign of the tail causes a zero in $d\sigma^R/dt$ and a dip in $d\sigma/dt$ located in the range 3–5 GeV^2. The rhs figure shows two examples of the dip structure, formed with $\beta_R = 1.10$ GeV^{-2} (solid line) and $\beta_R = 1.40$ GeV^{-2} (dashed line), as given in Table II. We suggest that the analysis of data from the Fermilab experiment at 1.96 TeV be extended to investigate this dip region.

To compare the BSW model with our calculations, we show in Fig. 6 the comparison of cross sections, and in Fig. 7 the comparison of amplitudes.

As shown in the left-hand size (lhs) plot, the amplitudes of the BSW model are qualitatively similar to ours in the low and mid $|t|$ ranges, with one imaginary and two real zeros, all of which occur at higher $|t|$ than ours. At higher $|t|$, shown in the rhs plot, important differences appear. In the BSW model, the imaginary magnitude dominates and falls to zero more slowly. In our case, the real part determines the tail behavior. At very large $|t|$ (namely $|t| \geq 6$ GeV^2), the roles of the imaginary and real magnitudes

FIG. 6.   Cross section comparison with BSW model. In the range 1–2 GeV^2, the BSW model has both real and imaginary amplitudes with magnitudes larger than ours (see Fig. 7), with consequence that the dotted line is higher.

are interchanged in comparison to ours. These qualitative similarities and differences of the two models have been observed also in the 7 TeV case [6].

V. SUMMARY AND DISCUSSION

In this work, we present precise descriptions of the elastic scattering amplitudes and of the differential cross sections for the $p\bar{p}$ collisions, merging the recent 1.96 TeV and the former 1.8 TeV data. We use analytical forms for the real and imaginary amplitudes covering the full $|t|$ range, identifying their zeros, signs, ranges of dominance, and the interplays that fix the observed details. To investigate the existing discrepancy of the 1.8 TeV data of the E-710 and CDF experiments in the presence of the new 1.96 TeV data, we construct three different combinations of data (called SETS I, II, and III) for the evaluation of total cross section and for the representation of the differential cross sections. Results are given in Tables I and II, and the solutions are illustrated in Figs. 1–3 for the data and in Fig. 4 for the amplitudes.

Figure 3 clearly shows how delicate the extrapolation of experimental data of $d\sigma/dt$ towards $|t| = 0$ is. Particularly, in the case where data points are lacking in the forward region, a more structured approach is fundamental for the determination of the so-called forward scattering parameters σ, ρ, B_I, and B_R, since they can only be defined in the limit $|t| \to 0$. Obviously, we cannot avoid model dependence, but we believe that the general features of the real and imaginary amplitudes, such as magnitudes, curvatures, zeros, and signs, are fundamental and should be incorporated in the analysis of the data. For example, the usually adopted assumption $B_R = B_I$ is essentially wrong and may lead to incorrect values for the forward scattering parameters.
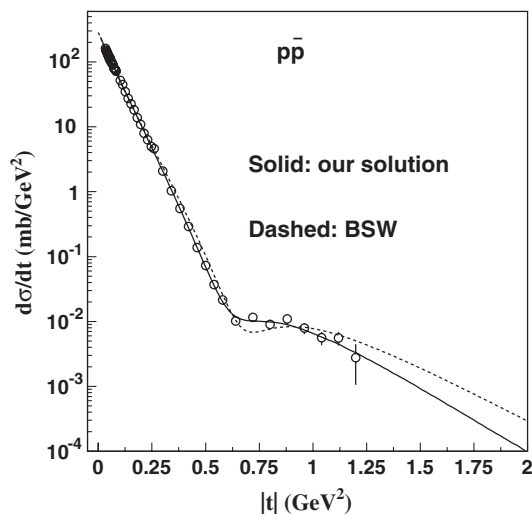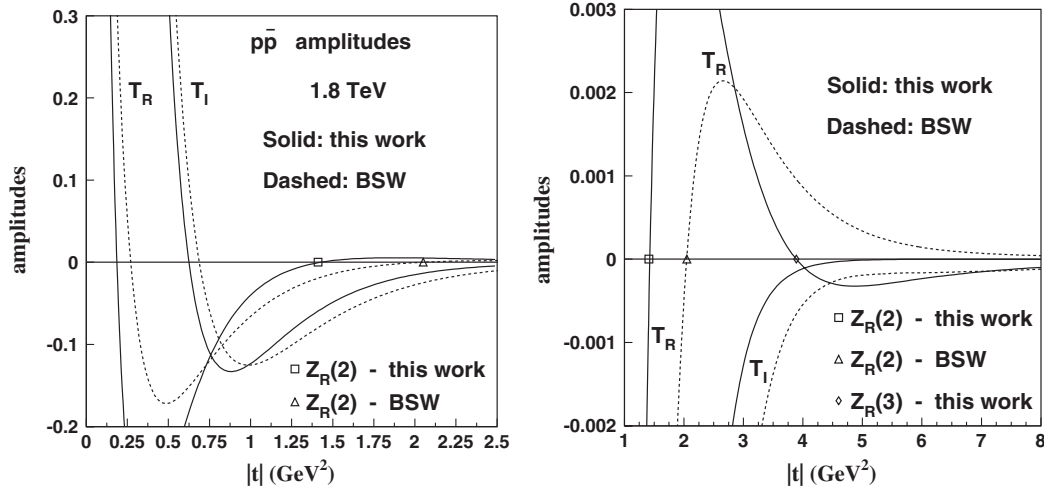
FIG. 7.   Comparison of BSW model amplitudes with ours. As shown in the lhs plot, the amplitudes of the BSW model are qualitatively similar to ours. In the rhs plot the vertical scale is amplified to illustrate the differences in the large $|t|$ domain.

Our work revises the values of total cross section and slope parameters that are reported in the literature, suggesting new values, which we believe to be more realistic. In addition, we show that with the use of the hybrid set combining CDF with large $|t|$ D0 data, the well-known discrepancy of CDF and E-710 data can be more tamed.

We show that, as is the cases of SPS and LHC energies [3,6], the universality of the perturbative three-gluon exchange tail as asymptotic behavior of the real part is consistent with the data and, in the particular p$\bar{\text{p}}$ case, leads to a very interesting consequence, due to the sign of this contribution. For $|t| > 4$ GeV^2, the nonperturbative real amplitude is positive and dominates the negative imaginary amplitude. The inclusion of the negative real contribution of the perturbative tail makes the real amplitude eventually negative again, creating a third zero. As the imaginary part is not dominant there, a marked dip may appear in $d\sigma/dt$ in this transition region as shown in Fig. 5. As mentioned in the text, the precise form of this dip structure depends on

the parameters which govern the behavior data in the transition region between nonperturbative and perturbative dominance.

The confirmation of the presence of this dip in the $3 \lesssim |t| \lesssim 4$ GeV^2 range would characterize the sign of the real amplitude and its dominance over the imaginary part in the mid t region, thus giving model-free information on the elastic scattering amplitude. We then propose the analysis of the collected data of the D0 collaboration at values of $|t|$ beyond those already published.

ACKNOWLEDGMENTS

[1] G. Antchev *et al.* (TOTEM Collaboration), Europhys. Lett. **95**, 41001 (2011); **96**, 21002 (2011); Report No. CERN-PH-EP-2012-239 (data extraction is available at the link, http://hepdata.cedar.ac.uk/view/red2659, Durham Data Basis; M. G. Ryskin, A. D. Martin, and V. A. Khoze, Eur. Phys. J. C **72**, 1937 (2012); I. M. Dremin and V. A. Nechitailo, Phys. Rev. D **85**, 074009 (2012).

[2] Auger Collaboration, Phys. Rev. Lett. **109**, 062002 (2012).

[3] E. Ferreira and F. Pereira, Phys. Rev. D **59**, 014008 (1998); **61**, 077507 (2000).

[4] H. G. Dosch, Phys. Lett. B **190**, 177 (1987); H. G. Dosch, E. Ferreira, and A. Kramer, Phys. Rev. D **50**, 1992 (1994).

[5] E. Ferreira, Int. J. Mod. Phys. E **16**, 2893 (2007).

[6] A. Kendi, E. Ferreira, and T. Kodama, Eur. Phys. J. C **73**, 2326 (2013).

[7] N. Amos *et al.* (Fermilab E-710 Collaboration), Phys. Lett. B **247**, 127 (1990).

[8] F. Abe *et al.* (Fermilab CDF Collaboration), Phys. Rev. D **50**, 5518 (1994).

[9] V. M. Abazov *et al.* (D0 Collaboration), Phys. Rev. D **86**, 012009 (2012).

[10] W. Faissler *et al.*, Phys. Rev. D **23**, 33 (1981).

[11] A. Donnachie and P. Landshoff, Z. Phys. C **2**, 55 (1979); Phys. Lett. B **387**, 637 (1996).

[12] V. Kundrát and M. Lokajicek, Phys. Lett. B **611**, 102 (2005); V. Kundrát, M. Lokajicek, and I. Vrococ, Phys. Lett. B **656**, 182 (2007); R. Cahn, Z. Phys. C **15**, 253 (1982); V. G. Gorshkov, E. Kuraev, L. Lipatov, and M. Nesterov, Zh. Eksp. Teor. Fiz. **60**, 1211 (1971) [Sov. Phys. JETP **33**, 655 (1971)].

[13] A. Martin, Phys. Lett. B **404**, 137 (1997).

[14] J. M. Cornwall, Phys. Rev. D **26**, 1453 (1982).

[15] S. Donnachie, G. Gosch, P. Landshoff, and O. Nachtmann, *Pomeron Physics and QCD* (Cambridge University Press, Cambridge, England, 2002).

[16] N. Amos *et al.*, Phys. Rev. Lett. **68**, 2433 (1992); C. Avila *et al.*, Phys. Lett. B **537**, 41 (2002).

[17] F. Abe *et al.*, Phys. Rev. D **50**, 5550 (1994).

[18] C. Bourrely, J. Soffer, and T. T. Wu, Eur. Phys. J. C **71**, 1601 (2011); C. Bourrely, J. M. Myers, J. Soffer, and T. T. Wu, Phys. Rev. D **85**, 096009 (2012).

[19] V. S. Fadin, E. Kuraev, and L. Lipatov, Phys. Lett. **60B**, 50 (1975); Zh. Eksp. Teor. Fiz. **72**, 377 (1977).